

Short Communication

## Fabrication of Pyrite FeS<sub>2</sub> Films from Electrochemically Deposited FeOOH by Sulfur Annealing

Sayaka Maki, Nobuaki Takeda, Masaya Ichimura\*

Department of Electrical and Mechanical Engineering, Nagoya Institute of Technology, Nagoya 466-8555, Japan

\*E-mail: [ichimura.masaya@nitech.ac.jp](mailto:ichimura.masaya@nitech.ac.jp)

Received: 29 June 2018 / Accepted: 7 August 2018 / Published: 1 October 2018

Pyrite (FeS<sub>2</sub>) thin films were fabricated via the sulfurization of electrochemically deposited  $\gamma$ -FeOOH. FeOOH thin films were deposited from an aqueous solution containing 50 mM FeSO<sub>4</sub> and 100 mM Na<sub>2</sub>SO<sub>4</sub>. The FeOOH precursor films and sulfur powder were placed in an alumina case with a lid, and annealed in N<sub>2</sub> at 400°C, 450°C, and 500°C for 30 min. For comparison, electrochemically deposited Fe–S–O films were also sulfurized under the same conditions. According to the Raman results, nearly phase-pure pyrite was obtained from the FeOOH precursor films, whereas a significant amount of marcasite phase was found in the films fabricated from the Fe–S–O precursor. Thus, phase-purity was greatly improved by adopting FeOOH as the precursor for pyrite.

**Keywords:** FeS<sub>2</sub>, pyrite, electrochemical deposition, FeOOH, sulfurization

### 1. INTRODUCTION

Pyrite (FeS<sub>2</sub>) is an earth-abundant and nontoxic mineral that has attracted considerable interest as a solar cell material because of its high optical absorption coefficient ( $\alpha \approx 5 \times 10^5 \text{ cm}^{-1}$ ) in the visible range and suitable bandgap (0.95 eV) [1]. Polycrystalline FeS<sub>2</sub> has been deposited by various methods, including chemical vapor deposition [2,3] and the sulfurization of iron thin films [4,5]. In addition, diodes based on FeS<sub>2</sub> nanoparticles have been fabricated by a few groups [6,7]. However, to date, no one has reported the successful fabrication of a pn junction solar cell based on FeS<sub>2</sub>. One possible reason for this is the presence of impurity phases such as marcasite (FeS<sub>2</sub>, orthorhombic crystal structure) and FeS. Thus, various strategies including laser annealing [8] and use of CoS<sub>2</sub> substrates [9] have been applied to remove impurity phases. Smestad et al. claimed that they successfully synthesized pure pyrite via the sulfurization of iron oxides (Fe<sub>2</sub>O<sub>3</sub> or Fe<sub>3</sub>O<sub>4</sub>) rather than elemental iron [10]. In conventional fabrication techniques, one must pass through the FeS phase field

in the Fe–S–O ternary phase diagram. In contrast, if Fe<sub>2</sub>O<sub>3</sub> or Fe<sub>3</sub>O<sub>4</sub> is sulfurized, the FeS field is not crossed, allowing impurity phases such as FeS to be diminished.

In this work, we deposit FeOOH films via electrochemical deposition (ECD), and then anneal these films in sulfur vapor. ECD is a low-cost technique for fabricating thin films, because it uses a simple apparatus and does not require a vacuum environment. Therefore, ECD is advantageous for solar cell production. ECD of  $\gamma$ -FeOOH thin films has been reported by our group [11]. To date, several groups have reported the fabrication of FeS<sub>2</sub> via the sulfurization of chemically deposited Fe–S–O precursors [12–15]. There are also a few reports of the sulfurization of chemically deposited iron oxide. Sun et al. fabricated FeS<sub>2</sub> films by sulfurizing Fe<sub>2</sub>O<sub>3</sub> films deposited by successive ionic layer adsorption and reaction [16]. Ouertani et al. synthesized FeS<sub>2</sub> from iron oxide films deposited by spray pyrolysis [17]. However, to the best of our knowledge, the fabrication of FeS<sub>2</sub> via the sulfurization of FeOOH has never been reported. For comparison, we also sulfurized ECD Fe–S–O precursor films. The results show that phase purity is greatly improved when FeOOH is adopted as the precursor.

## 2. EXPERIMENTAL

Our ECD apparatus is a three-electrode system with a fluorine-doped tin oxide (FTO)-coated glass substrate as the working electrode, a platinum sheet as the counter electrode, and an Ag/AgCl electrode as the reference electrode.  $\gamma$ -FeOOH thin films were deposited on an FTO substrate by ECD at room temperature from an aqueous solution containing 50 mM FeSO<sub>4</sub> and 100 mM Na<sub>2</sub>SO<sub>4</sub> [11]. The solution was saturated with oxygen by gas bubbling before the start of deposition. The deposition current density was kept at a constant value of  $-0.32 \text{ mA/cm}^2$ . The deposition time was 10 min. For comparison, Fe–S–O thin films were also fabricated by ECD. Fe–S–O thin films were deposited from an aqueous solution containing 50 mM FeSO<sub>4</sub> and 100 mM Na<sub>2</sub>S<sub>2</sub>O<sub>3</sub> at 15°C [18,19]. The deposition current and time were  $-1.5 \text{ mA/cm}^2$  and 60 s, respectively. Sulfur powder was placed on the surface of the FeOOH and Fe–S–O films, and the films were then placed in an alumina case with a lid followed by annealing in N<sub>2</sub> at 400°C, 450°C, and 500°C for 30 min. The introduction of N<sub>2</sub> can improve temperature uniformity in the annealing furnace and prevent the effusion of sulfur vapor from the case. Scanning electron microscopy (SEM) images and the elemental compositions obtained via Auger electron spectroscopy (AES) were collected using a JEOL JAMP-9500F field emission microprobe at a probe voltage of 10 keV. Before measurement, contaminants were removed from the thin-film surface by Ar ion etching. Optical transmittance was measured using a V-570 double-beam spectrophotometer (JASCO). X-ray diffraction (XRD) patterns were recorded using a SmartLab X-ray diffractometer (Rigaku) with CuK $\alpha$  radiation. Raman spectra excited by a 632.8 nm He–Ne laser were collected using a JASCO NRS 3300 spectrometer.

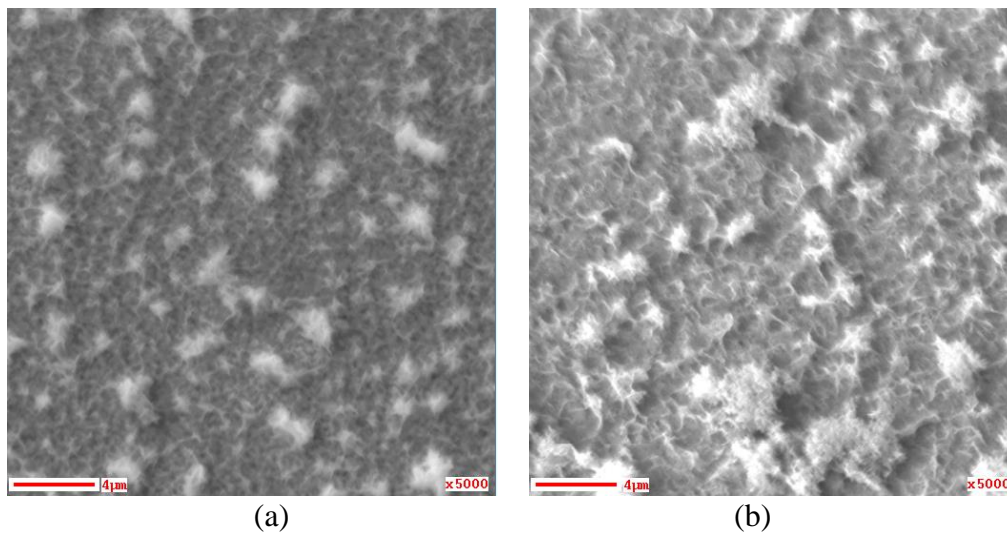


**Figure 1.** SEM images of (a) the as-deposited FeOOH film, and (b) the FeOOH film sulfur-annealed at 450°C.

### 3. RESULTS AND DISCUSSION

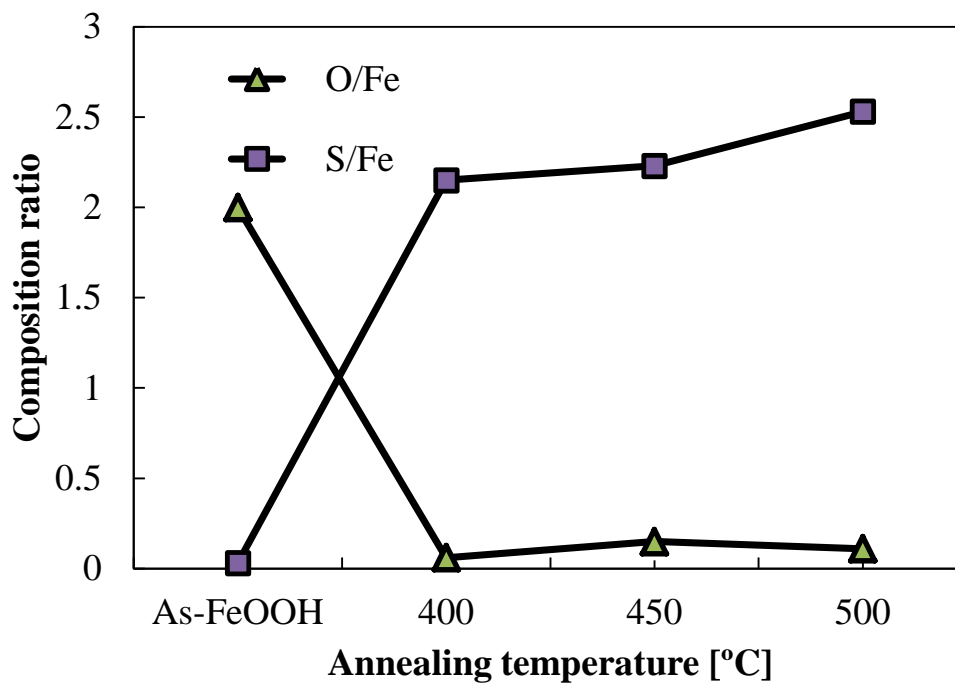


**Figure 2.** Elemental composition ratios of the as-deposited and annealed (sulfurized) FeOOH films as a function of the annealing temperature.

The as-deposited  $\gamma$ -FeOOH film was yellow in color and had a thickness of 0.25 – 0.5  $\mu\text{m}$  (the thickness uniformity within the deposition area was rather poor). On the other hand, the color of the Fe–S–O film was black, and its thickness was approximately 0.2  $\mu\text{m}$ .

After sulfur annealing, the color of the FeOOH film changed from yellow to black. The film thickness did not change significantly after annealing, regardless whether the FeOOH or Fe–S–O precursor film was used. Figure 1 shows SEM images ( $\times 5000$ ) of the as-deposited FeOOH film and film annealed at 450°C. The as-deposited film exhibited flake-like surface morphology, and no significant change in morphology was observed after the sulfur annealing.

The elemental composition ratios of the as-deposited and annealed FeOOH films were calculated from the AES data and are plotted in Fig. 2 as a function of the annealing temperature. Annealing at 400–500°C caused the S/Fe ratio to increase from null to approximately 2.2, while the O/Fe ratio decreased from 2.0 to approximately 0.15. The dependence of elemental composition on annealing temperature was not significant in this temperature range. For the Fe–S–O sample, O/Fe and S/Fe ratios before annealing were 0.66 and 1.47, respectively. Thus, the film contained comparable amounts of oxygen and sulfur. After annealing at 450°C, O/Fe was decreased to 0.08, and S/Fe was increased to 2.7. These results show that we successfully sulfurized both the FeOOH and Fe–S–O precursors. The S/Fe ratio after the sulfurization was larger than the stoichiometric ratio (2). This can be partly attributed to an inaccurate estimate of the relative sensitivity for each element. We used commercial FeS as a standard reference sample in the composition calculations, but the actual S/Fe ratio of the standard sample may be smaller than the nominal value because of sulfur evaporation and oxidation. Thus, the sensitivity of sulfur along with the S/Fe ratio were overestimated.

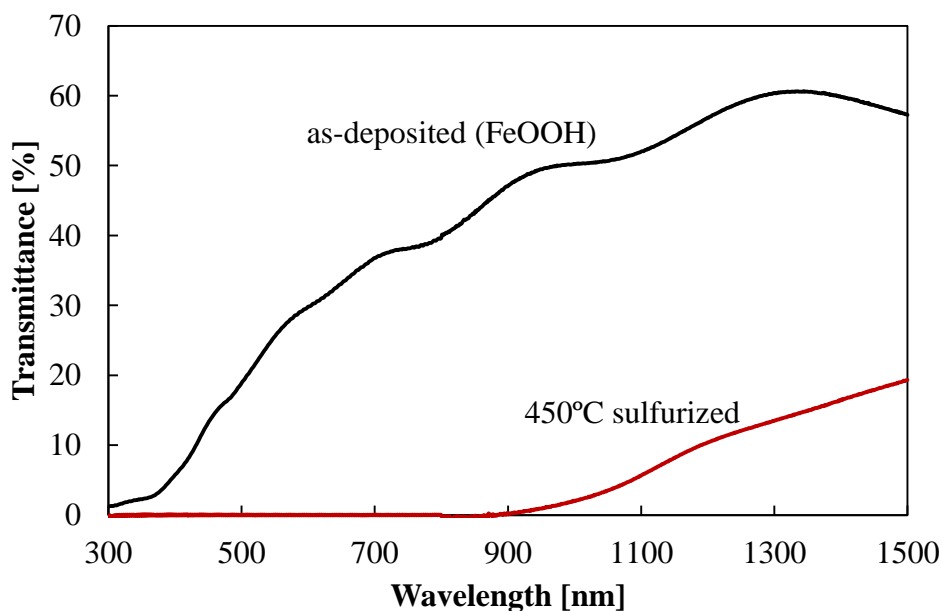


**Figure 3.** Optical transmittance of the FeOOH films before and after sulfurization at 450°C.

Figure 3 shows the optical transmission spectra of the as-deposited FeOOH film and the film sulfurized at 450°C. Before sulfurization, the film transmission exceeded 30% in the red–yellow wavelength range (the film was yellow in color, as stated above). After sulfurization, the transmission in the visible range was 0% (the film became black). No clear absorption edge was observed; thus, the band gap could not be accurately evaluated. However, the band gap may be regarded as less than 1.2

eV since the transmission is small for wavelengths below 1  $\mu\text{m}$ . The films sulfurized at 400°C and 500°C showed transmission curves similar to that of the sample sulfurized at 450°C.

In the XRD patterns of the as-deposited FeOOH and Fe-S-O films, only peaks of the FTO substrate were observed. Thus, the as-deposited films are considered to be amorphous. Figure 4 shows the XRD pattern of the FeOOH sample sulfurized at 450°C. Several peaks of pyrite can be observed, as indexed in Figure 4. However, because of the poor signal-to-noise ratio, the peak position could not be accurately evaluated. The XRD peaks of marcasite are positioned close to those of pyrite. Therefore, it is difficult to determine whether the FeS<sub>2</sub> phase is pyrite or marcasite from the XRD data.

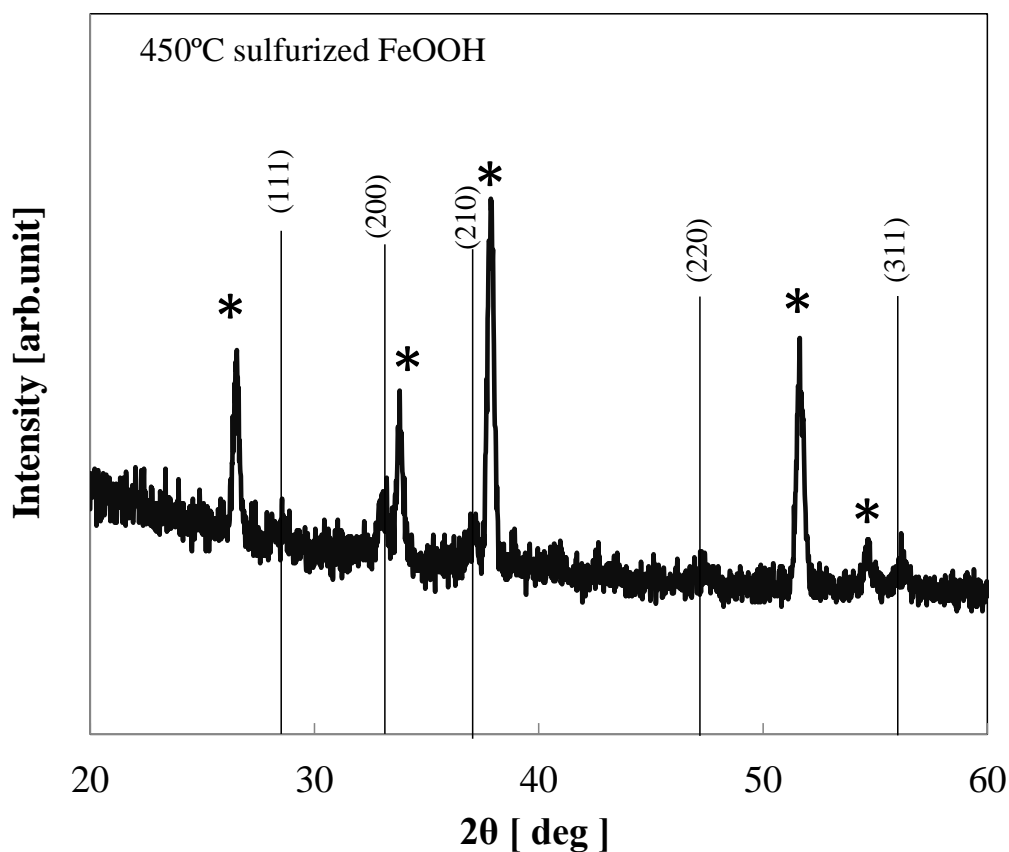


**Figure 4.** XRD pattern of the FeOOH film sulfurized at 450°C. The peaks of pyrite are indexed, and the peaks of FTO are labeled with \*.

Figure 5 shows the Raman spectra of the fabricated samples. Two peaks at 251 and 386  $\text{cm}^{-1}$  and one broad peak at approximately 309  $\text{cm}^{-1}$  are observed in the spectrum of the as-deposited FeOOH film. These peaks are characteristic of  $\gamma$ -FeOOH [20]. In the spectrum of the as-deposited Fe-S-O, all the observed peaks are broad and shifted compared to those reported for the pure compounds. Pyrite was reported to exhibit two dominant peaks at 340 and 380  $\text{cm}^{-1}$  along with an additional weak peak at 425  $\text{cm}^{-1}$  [21]. These main pyrite peaks are clearly observed in the spectrum of the sulfurized Fe-S-O sample (the bottom spectrum in Figure 5), but another dominant peak corresponding to marcasite also appears at 330  $\text{cm}^{-1}$  [22]. The asymmetry of the peak at 380  $\text{cm}^{-1}$  is attributed to overlap with a slightly blue-shifted peak that is also indexed to marcasite. Therefore, the sulfurized Fe-

S–O sample contained a significant amount of marcasite in addition to pyrite. In contrast, the Raman spectra of the sulfurized FeOOH films are similar to the reported spectrum of pyrite. The small hump around  $330\text{ cm}^{-1}$  in the spectrum of the sample sulfurized at  $450^\circ\text{C}$  can be attributed to marcasite. However, the intensity of this peak is much smaller than that of the dominant marcasite peak in the sulfurized Fe–S–O sample. The spectrum of the FeOOH sample sulfurized at  $400^\circ\text{C}$  is similar to that of the FeOOH sample sulfurized at  $450^\circ\text{C}$ .

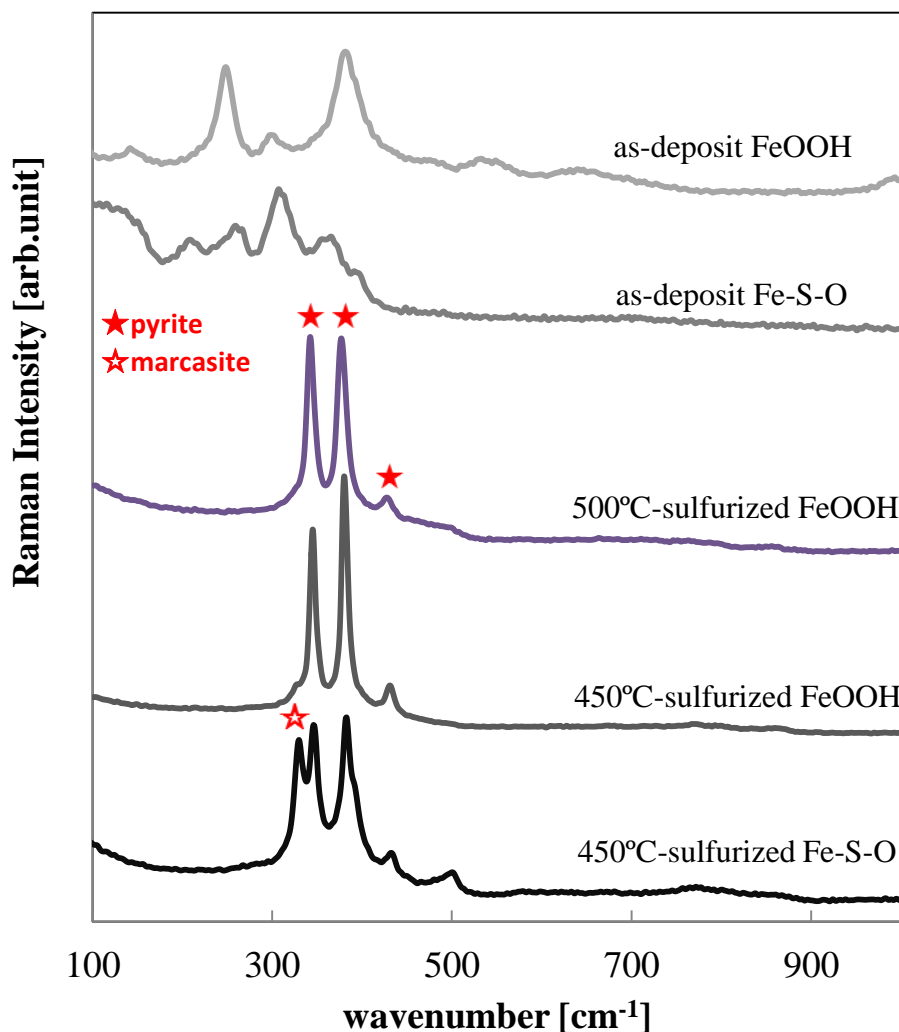


**Figure 5.** Raman spectra of the as-deposited and sulfurized samples.

The above results indicate that better FeS<sub>2</sub> phase purity was obtained when FeOOH was used as the precursor material rather than Fe–S–O. As noted in the introduction, in most previous attempts to synthesize FeS<sub>2</sub> from chemically deposited precursors, the precursor contained both O and S [12-15]. We do not understand exactly how the precursor material influences the phase purity after sulfurization. However, we speculate that chemical disorder in the precursor could affect film crystallinity after sulfurization. In other material systems, chemical disorder and the local atomic environment are known

to influence phase transition behavior [23-25]. Furthermore, alloy composition can affect the temperature and incubation time of crystallization by changing the bonding energy or relieving local stress. In this study, both the FeOOH and Fe-S-O precursors were amorphous; however, unlike the FeOOH precursor, the Fe-S-O precursor exhibits chemical disorder in addition to structural disorder. This chemical disorder may prevent the film from forming well-ordered crystalline phase, and the poor crystallinity may lead to a mixture of crystalline phases after sulfurization.

#### 4. SUMMARY

In this work, we synthesized pyrite from ECD FeOOH precursor films for the first time. The FeOOH films were electrochemically deposited from a solution containing FeSO<sub>4</sub> and Na<sub>2</sub>SO<sub>4</sub>. The as-deposited FeOOH film was yellow in color and then turned black after sulfurization at 400°C–500°C. The peak corresponding to pyrite was clearly observed in the Raman spectra of the sulfurized samples, while the marcasite peak was almost negligible. For comparison, Fe-S-O films were also electrochemically deposited from a solution containing FeSO<sub>4</sub> and Na<sub>2</sub>S<sub>2</sub>O<sub>3</sub> and sulfurized under the same conditions. In the Raman spectra of the sulfurized Fe-S-O samples, the intensity of the marcasite peak was comparable to that of the pyrite peak. Thus, the phase purity was superior when FeOOH was used as the precursor instead of Fe-S-O.

This work was partly supported by Iketani Science and Technology Foundation.

#### References

1. A. Ennaoui and H. Tributsch, *Solar Cells*, 13 (1984) 197.
2. D. M. Schleich and H. S. W. Chang, , 112 (1991) 737.
3. J. Oertel, K. Ellmer, W. Bohne, J. Röhrich, and H. Tributsch, *J. Cryst. Growth* 198–199, 1205 (1999).
4. L. Meng, J. P. Tu, and M. S. Liu, *Mater. Lett.*, 38 (1999) 103.
5. I. J. Ferrer and C. Sanchez, *J. Appl. Phys.*, 70 (1991) 2641.
6. D. Wang, Y. Jiang, C. Lin, S. Li, Y. Wang, C. Chen, and C. Chen, *Adv. Mater.*, 24 (2012) 3415.
7. D. G. Moon, A. Cho, J. H. Park, S. H. Ahn, H. S. Kwon, Y. S. Cho, and S. Ahn, *J. Mater. Chem. A*, 2 (2014) 17779.
8. M. Umehara, Y. Takeda, H. Azuma, T. Motohiro, *Jpn J. Appl. Phys.*, 51 (2012) 02BP10.
9. L. Samad, M. Caban-Acevedo, M. J. Shearer, K. Park, R. J. Hamers, and S. Jin, *Chem. Mater.*, 27 (2015) 3108.
10. G. Smestad, A. Ennaoui, S. Fiechter, H. Tributsch, W.K.Hofmann, M. Birkholz, and W. Kautek, *Solar Energy Mater.*, 20 (1990) 149.
11. J.J. M. Vequizo and M. Ichimura, *Appl. Phys. Express*, 6 (2013) 125501.
12. D. A. D. A. Maz'on-Montijo, M. T. S. Nair, and P. K. Nair, *ECS J. Solid State Sci. Technol.*, 2 (2013) P465.
13. A. Gomes, J.R. Ares, I.J. Ferrer, M.I. da Silva Pereira, and C. Sa'nchez, *Mater. Res. Bull.*, 38 (2003) 1123.

14. S. Nakamura and A. Yamamoto, *Sol. Energy Mater. Sol. Cells*, 65 (2001) 79.
15. S. Kawai, T. Kajima, M. Ichimura, *Mater. Res. Express*, 3 (2016) 025901.
16. K. Sun, Z. Su, J. Yang, Z. Han, F. Liu, Y. Lai, J. Li, and Y. Liu, *Thin Solid Films*, 542 (2013) 123.
17. B. Ouertania, J. Ouerfellib, M. Saadouna, B. BessaRsa, M. Hajjia, M. Kanzaric, H. Ezzaouiaa, N. Hamdadoud, J.C. Berne` de, *Mater. Lett.*, 59 (2005) 734.
18. S. Kawai, R. Yamazaki, S. Sobue, E. Okuno, and M. Ichimura, *APL Mater*, 2 (2014) 032110.
19. K. Yang, S. Kawai, and M. Ichimura, *Thin Solid Films*, 573 (2014) 1.
20. D. L. A. de Faria, S. Venancio Silva, and M. T. de Oliveira, *J. Raman Spectrosc.*, 28 (1997) 873.
21. H. Vogt, T. Chattopadhyay, and H. J. Stolz, *J. Phys. Chem. Solids*, 44 (1983) 869.
22. C. Sourisseau, R. Cavagnat, and M. Fouassier, *J. Phys. Chem. Solids*, 52 (1991) 537.
23. O. H. Roh, W. J. Yun, and J.-K. Lee, *J. Appl. Phys.*, 90 (2001) 2786.
24. A. V. Sapelkin, S. C. Bayliss, A. G. Lyapin, and V. V. Brazhkin, *Phys. Rev. B*, 61 (2000) 1907.
25. R. Aravinda Narayanan, S. Asokan, and A. Kumar, *Phys. Rev. B*, 63 (2001) 092203.

© 2018 The Authors. Published by ESG ([www.electrochemsci.org](http://www.electrochemsci.org)). This article is an open access article distributed under the terms and conditions of the Creative Commons Attribution license (<http://creativecommons.org/licenses/by/4.0/>).